

Three-dimensional Finite Element Stress Analysis of a Cuneiform-Geometry Implant

Mauro Cruz, DDS, MDSci¹/Thomaz Wassall, DDS, MDSci, PhD²/Elson Magalhães Toledo, Eng, MSc, DSc³/
Luis Paulo da Silva Barra, Eng, MSc, DSc⁴/Afonso Celso de Castro Lemonge, Eng, MSc, DSc⁴

Purpose: The biomechanical behavior of an osseointegrated dental implant plays an important role in its functional longevity inside the bone. Studies of this aspect of dental implants by the finite element method are ongoing. In the present study, a cuneiform-geometry implant was considered with a 3-dimensional model that had a mesh that was finer than in the models commonly found in the literature. **Materials and Methods:** A mechanical model of an edentulous mandible was generated from computerized tomography, with the implant placed in the left first premolar region. A 100-N axial load was applied at the implant abutment, and the mandibular boundary conditions were modeled considering the real geometry of its muscle supporting system. The cortical and trabecular bone was assumed to be homogeneous, isotropic, and linearly elastic. **Results:** The stress analysis provided results that were used to plot global and detailed graphics of normal maximum (S1), minimum (S3), and von Mises stress fields. The results obtained were analyzed and compared qualitatively with the literature. **Discussion:** Quantitative comparisons were not performed because of basic differences between the model adopted here and those used by other authors. The stress distribution pattern for the studied geometry was similar to those found in the current literature, but insignificant apical stress concentration occurred. The stress concentration occurred at the neck of the implant, ie, in the cortical bone, which was similar to results for other implant shapes reported in the literature. **Conclusion:** The studied geometry showed a smooth stress pattern, with stress concentrated in the cervical region. The values, however, were within the range of values found in the cortical layer far from the implant, caused by the muscular action. No significant stress concentration was found in the apical area. (More than 50 references.) INT J ORAL MAXILLOFAC IMPLANTS 2003;18:675–684

Key words: biomechanics, dental implants, dental stress analysis, finite element analysis

¹Director, Clinical Center of Research in Stomatology, Juiz de Fora, MG, Brazil.

²Director, Department of Postgraduate Dentistry, Unicastelo, Camilo Castelo Branco University, Ponte Preta, Campinas, SP, Brazil.

³Researcher, Computational Mechanics Coordination, National Laboratory for Scientific Computing, Petrópolis, RJ, Brazil; Professor, Federal University of Juiz de Fora (UFJF), School of Engineering, Campus Cidade Universitária, Juiz de Fora, MG, Brazil.

⁴Professor, UFJF, School of Engineering, Campus Cidade Universitária, Juiz de Fora, MG, Brazil.

Reprint requests: Dr Mauro Cruz, Clinical Center of Research in Stomatology, Av. Rio Branco 2288/1205, Juiz de Fora, MG, CEP 36016901, Brazil. Phone/Fax: + 55-32-3215-3957. E-mail: clinest@terra.com.br

This article was based on a Master of Science thesis submitted by Dr Mauro Cruz to Camilo Castelo Branco University, October 2001, Campinas, SP, Brazil.

Dental implants are frequently submitted to multidirectional loads originating in the stomatognathic system,^{1–5} and the bone stress distribution pattern is highly relevant to the bone-implant relationship and consequently to its longevity.^{3–7} The biomechanical behavior is directly dependent not only on the implant geometry, but on the whole design of the implant, which includes its shape and material, as well as the prosthesis it supports.^{8,9} Considering the similarity of prostheses and materials in all prosthetic solutions, valuable contributions may come through the study of the influence of implant shape.⁸ Mechanical analysis using the finite element method (FEM) has been employed by many authors to understand the biomechanical behavior around dental implants^{3,6,10–37} with a suitable degree of reliability and accuracy, but without the risk and expense of implantation.³

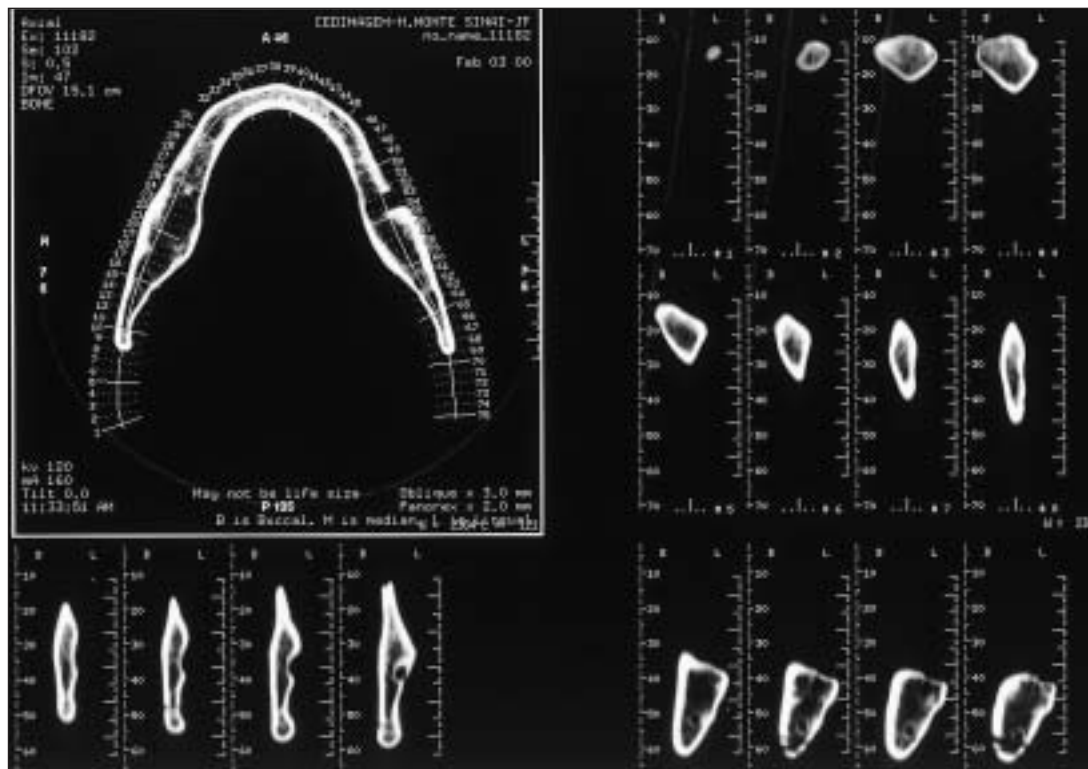


Fig 1 To begin creating the model used for FEM in this study, CT of the mandible was performed.

The degree of accuracy of the FEM is related to knowledge of the real load and supporting conditions.³⁸⁻⁴³ Different studies agree that biomechanical behavior plays an important role in the survival of an implant,^{3-7,10,28-30,44} that geometry is a key factor associated with stress distribution,^{5,13,45,46} and that the FEM can be a reliable method for studying the biomechanical behavior of implants.^{3,5-7,14,15,26,28,37,39} Previous attempts to model the tissue-implant interaction have, for the most part, been limited to the use of 2-dimensional (2D) analysis,^{5,7,10,13} and more refined models that bear a closer resemblance to actual anatomic and physiologic structures can make the method's results more reliable.^{38,39,43} The influence of environmental conditions around the implant, such as different degrees of bone-implant contact,^{6,11} presence of cortical or cancellous bone,^{21,23} and mandibular body deformation,⁴⁷ have also been studied and reproduced.^{3,6,14,15,28,44}

The osseointegrated implant interface is rigid and transmits occlusal loads directly to adjacent bone. This condition can produce high levels of stress,⁴⁸ concentrated mainly in the neck and apex region,⁴⁹⁻⁵² that can affect the bone physiology.^{53,54} Many authors have studied and tried to develop different ways to compensate this situation through the use of devices such as an intramobile element^{29,55,56} or a resilient collar around the implant neck⁵⁷ and

even with cementum/periodontal ligament formation around the implant.⁵⁸⁻⁶⁰ Different geometries have been studied, and attempts have also been made toward shape optimization that enhances the relationship between bone and implant, allowing for improved biomechanical performance.^{27,29,30}

The goal of this work was to analyze the stress distribution around a cuneiform implant using accurate modeling capable of obtaining more precise data, thereby enhancing the results found in the current literature.

MATERIALS AND METHODS

The starting point of this study was the development of an accurate model of an edentulous mandible, which was essential for obtaining more precise results.^{38,39,43}

Geometric Modeling

Initially, computerized tomography (CT) (Tomograph Pro-Speed; GE Medical Systems, Fairfield, CT) of an actual human mandible was obtained according to the description of Inou and coworkers⁴³ (Fig 1). With the help of a scanner, the images obtained were converted into digital data and transferred to a CAD program (AutoCAD; Autodesk, San

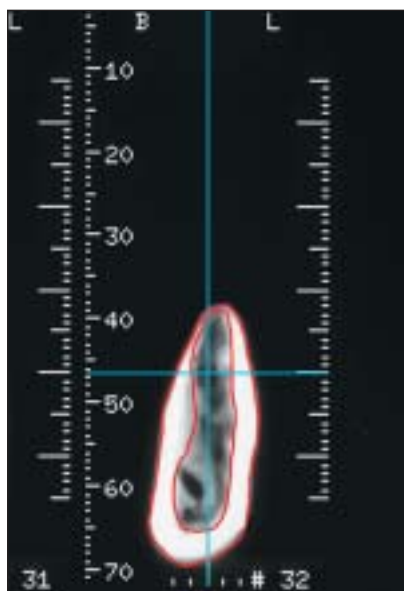


Fig 2a Transverse section #32, where the implant was placed.

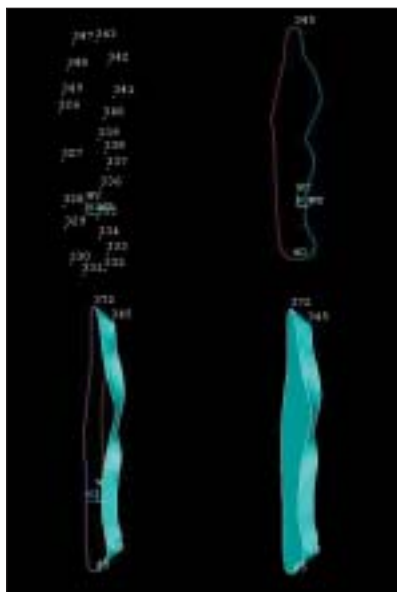


Fig 2b Assembly of the geometric model, the points, lines, surfaces, and volumes.



Fig 2c Computational geometric model of the mandible.

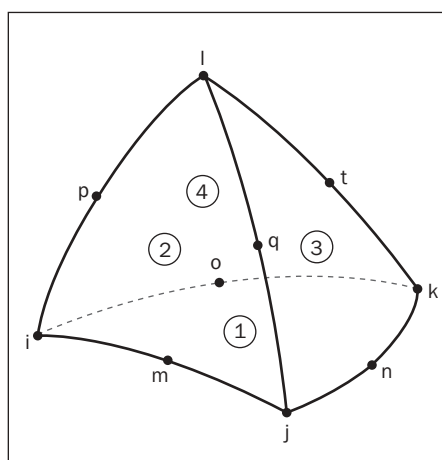


Fig 3 (Left) Tetrahedral isoparametric square element.

Fig 4 (Below) Mathematical model of the mandible showing the finite element mesh.



Rafael, CA), where the coordinates of the contouring points were extracted from these plots and joined to form partial volumes that together defined the final geometry (Figs 2a and 2b). This sequence was done on one side and repeated to obtain the other side. Through this process the CT data were converted into a 3D solid model (Fig 2c).

Mathematical Modeling

As is routine when using FEM, the geometric model was meshed; in the present case, this was done with tetrahedral isoparametric quadratic elements, utilizing 4 triangular faces, 4 vertices, and 10 nodes (Fig 3). The displacement of these nodes was found and used in the calculation of the stress distribution inside the structure. The grid reached 85,800 elements with 362,610 degrees of freedom.

Of this total number of elements, 67,120 of them, which corresponded to 276,960 degrees of freedom, were distributed in the region of the left premolar, between sections #30 and #34 where the implant was placed (Fig 2a), since the greatest numeric accuracy was desired in this area. The remaining elements were distributed throughout the mandibular body (Fig 4). The Bioform implant (Maxtron, Juiz de Fora, MG, Brazil) was modeled by a CAD program (Fig 5a) together with its prosthetic abutment in a fine mesh (Fig 5b) with 17,193 elements and 80,134 degrees of freedom (Table 1).

Load and Supporting System

For the boundary condition of the model, a supporting system was set up. The model was supported by the muscles of mastication³⁵ and the

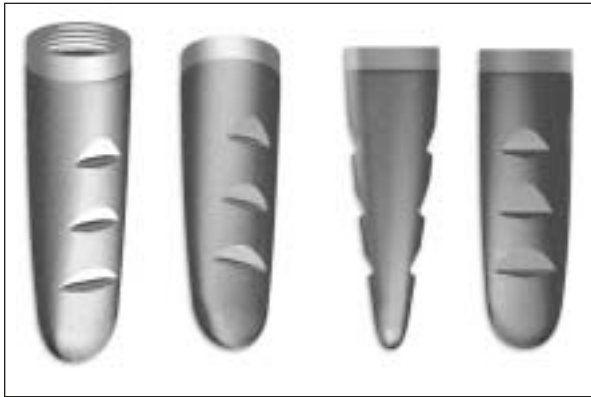


Fig 5a Views of the Bioform implant with its cuneiform geometry. It has 3 notches on each major side of the body to enhance mechanical retention.

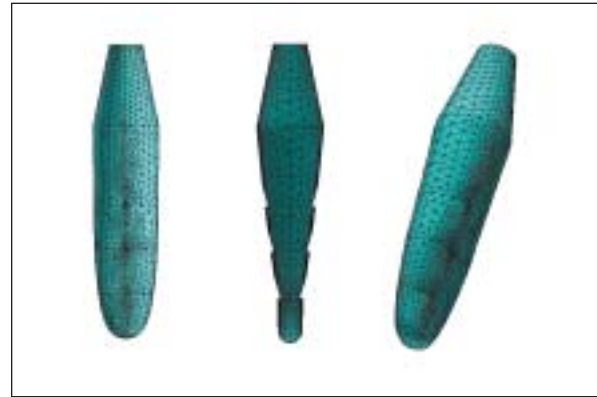


Fig 5b Mathematical model of the Bioform implant 413 and the abutment.

Table 1 Mesh Data			
Region	Elements	Nodes	Degrees of freedom
Implant/abutment	17,193	26,708	80,134
Sections 30 to 34 + implant/abutment	67,120	92,320	276,960
Complete model	85,800	120,870	362,610

Table 2 Distance Vector Components (mm)			
Vector distance	X direction	Y direction	Z direction
r_M	0.0	28.07	33.01
r_T	0.0	30.61	5.27
r_{PL}	0.0	9.56	6.31
r_{PM}	0.0	27.67	38.97
r_{P_0}	0.0	80.63	23.89

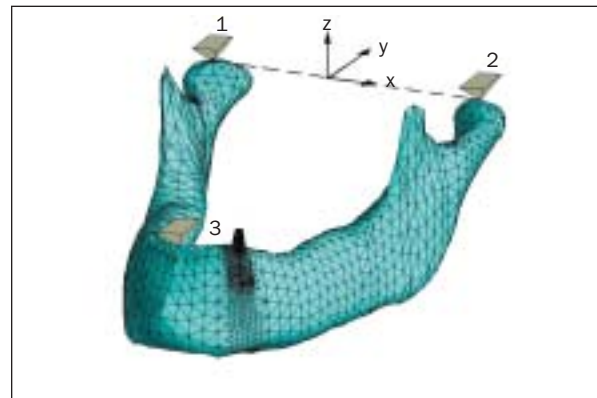


Fig 6 Model with restraining adopted. Point 1 = Translation restrained in directions x, y, z; point 2 = translation restrained in directions y, z; point 3 = check point.

temporomandibular joints.⁶¹ The forces generated by the muscles of mastication (temporalis [T], masseter [M], medial pterygoid [PM], and lateral pterygoid [PL]) were calculated, based on their transverse sections, according to Inou and coworkers.⁴³ Adapting the data from this reference, the relationships between the muscle actions were as follows:

$$M = 1.72 PL \quad (\text{equation 1})$$

$$T = 0.99 PL \quad (\text{equation 2})$$

$$PM = 1.15 PL \quad (\text{equation 3})$$

The model was restrained as shown in Fig 6, and an axial load $P_0 = 100$ N was applied at the top of the abutment. The values of the muscular forces to keep the model equilibrated were obtained from the following equation.

$$2M \times r_M + 2PM \times r_{PM} + 2PL \times r_{PL} + 2T \times r_T + 100\mathbf{u} \times r_P = 0 \quad (\text{equation 4})$$

where r_M , r_{PM} , r_{PL} , r_T , and r_P are the distance vectors from the load application points of the M, PM, PL, T, and P_0 (axial load over the implant) to the x (1-2) axis, that pass across the center of the condyles, respectively (Fig 6). In this equation, the symbol \mathbf{u} indicates the unitary vector in the implant axis direction and the symbol \times denotes the vector product.

The positions of the vectors of the muscular forces and the axial load are indicated in Table 2.

The muscle positioning on the mandibular body (Fig 7a) was approximated based on descriptions found in the literature,⁶²⁻⁶⁶ and the results of the muscular forces were considered to be acting on the centroid of the nodes of the elements that define the muscular action areas⁶⁷ (Fig 7b).

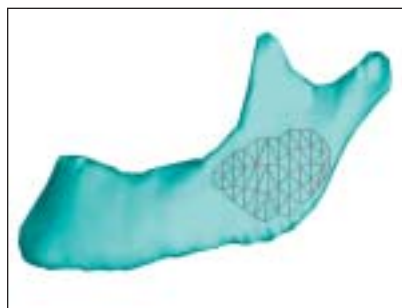


Fig 7a Outline of distribution of the masseter muscle.

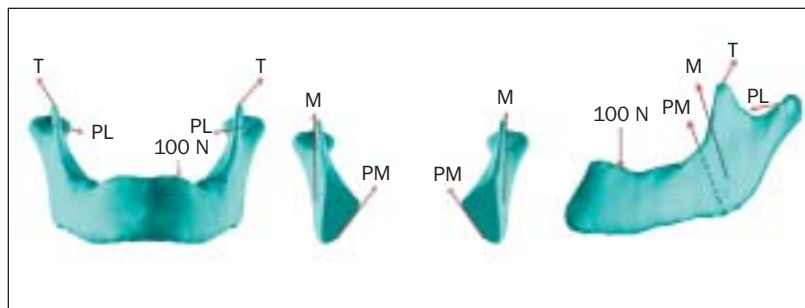


Fig 7b Directions of the applied muscular forces.

Table 3 Directional Cosines of the Resultant Muscular Forces (Right Side)

Muscle	Cos (α)	Cos (β)	Cos (γ)
Masseter	-0.043	-0.011	0.999
Medial pterygoid	0.587	-0.165	0.792
Lateral pterygoid	0.714	-0.692	0.106
Temporalis	-0.325	0.219	0.920

Table 4 Elasticity of Materials Used

Material	Modulus elasticity	Poisson's ratio	References
Cortical bone	13,700 MPa	0.30	3,6,11,16,21-25, 27,28,44,46,50
Cancellous bone	1,370 MPa	0.30	11,16,21,23-25, 28,44,46
Titanium	110,000 MPa	0.33	16,22,25,26

The directions of the forces were established by the cosine extracted from the geometry considered (see Table 3).

Equation 4 and the relationships described led to the resultant values, which were: M = 59.23 N; PM = 39.60 N; PL = 34.44 N; and T = 34.09 N.

Material Properties

In the absence of information about the bone's precise material properties, assumptions were made according to the majority of studies that used FEM (Table 4).

The areas of cortical and cancellous bone were assumed as defined by the CT sections in the mandibular body (Fig 2), and the 2 types of bone modeled (cortical and cancellous) were considered isotropic, homogeneous, and linearly elastic.

Implant System, Load Positioning, and Interface Conditions

The cuneiform implant used here is 13 mm long and 4 mm in diameter (Figs 5a and 5b). This geometry has an interesting resemblance to natural roots^{68,69} and also has a high degree of applicability because of its bone-induced expansion capacity.⁷⁰ Its design also presents 3 notches on each side of the body, which provides better mechanical retention during prosthetic management. The dimensions were chosen according to the majority of FEM studies. It was assumed that the implant was placed between sections #30 and #34, ie, the premolar region, which is

representative of the average force acting in the mouth.^{8,39} A vertical load of 100 N was applied on top of the abutment in the direction of the long axis of the implant.^{17,28,32,44} A layer of cortical bone 2 mm thick was contoured around the implant neck, and the body of the implant was embedded in the cancellous bone. A fixed bond, ie, total osseointegration, between bone and implant along the whole interface was assumed, which meant that under the applied load on the implant, relative motion between bone and implant did not occur.

Operational Conditions

The analyses were accomplished with the Ansys software program (Ansys Corporate, Canonsburg, PA) and processed by a personal computer (IBM, White Plains, NY).

RESULTS

The stress analysis executed by Ansys provided results that enabled the tracing of global and detailed graphics of the maximum (S1) and minimum (S3) principal stresses and the von Mises stress field. Stress contours were color-coded and explained for each figure. All stress values were indicated in mega pascals (MPa).

Figures 8a to 8d display the global results as the mandibular body deformation presented a medial convergence⁴⁷ (Fig 8a). The maximum and minimum

Fig 8 Global results.

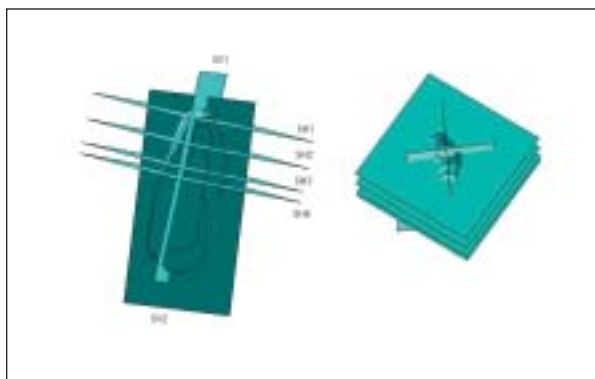
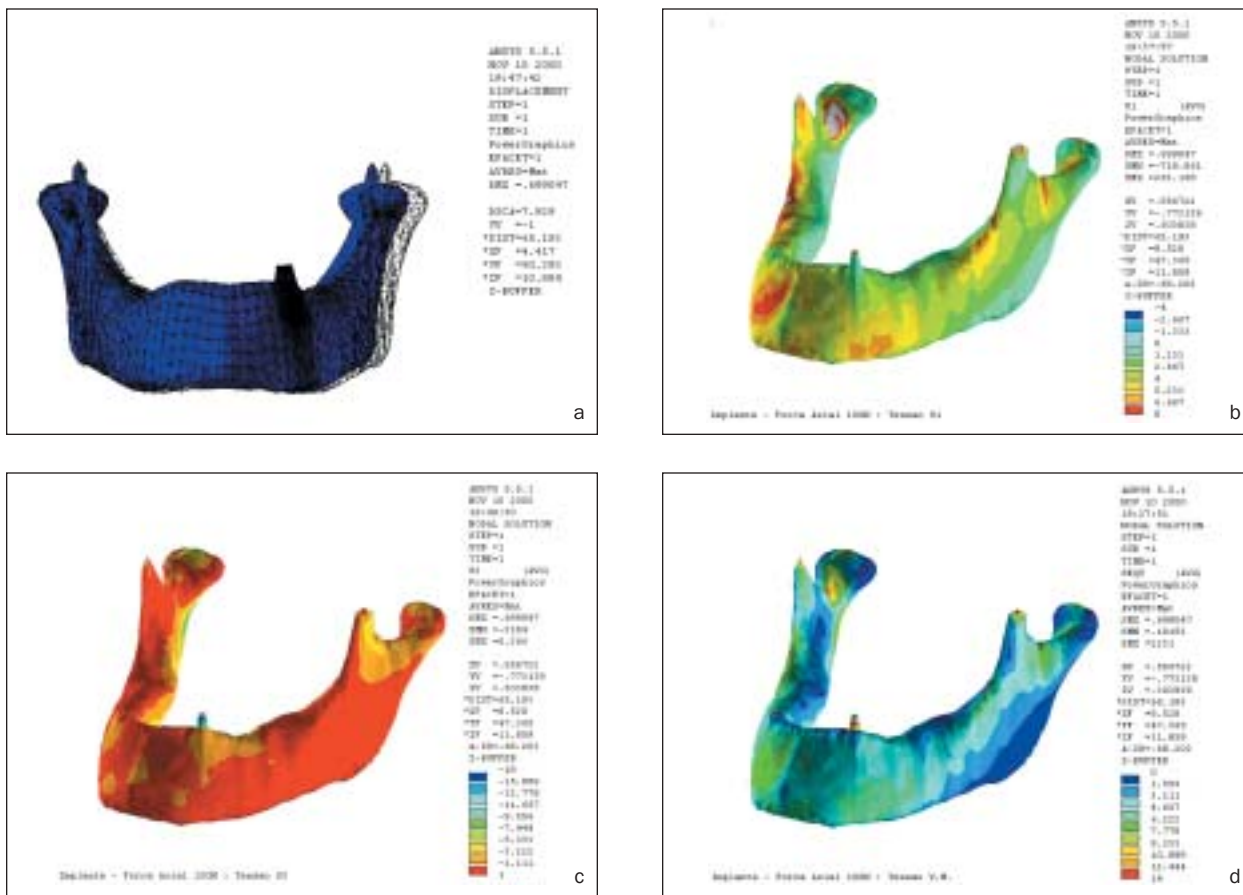


Fig 9 Positioning of the horizontal and vertical sections.

principal stresses showed smooth distribution, with stress concentration only at the muscular insertions (Figs 8b and 8c); the same occurred with the von Mises criteria stresses (Fig 8d).

For enhanced accuracy, analysis graphics were made of the region between the sections #30 and #40

to show the values of principal maximum, minimum, and von Mises criteria stresses. The images were presented in 4 transverse and 2 longitudinal sections (Fig 9) and 2 more detailed sections from the implant's neck region (Figs 10a to 10c). The transverse sections were obtained as follows: SH4 is tangent to the apex of the implant, SH3 is 2 mm from SH4, SH2 is 4.5 mm from SH3, and SH1 is 5 mm from SH2.

All graphics showed a smooth distribution of stresses, with no significant concentration at the apex. An area of stress concentration was present on one side of the neck. However, the values were equivalent to those registered at the insertion of the masseter. The highest stress concentration occurred at the superior side of the cortical layer, but the values shown within the figures were within the same order of those encountered in the cortical layer under the masseter. Low areas of stress were observed on the upper side of the re-entrances (Figs 10a to 10c) present in the implant body but were within the bony physiologic limits. The cross sections showed stresses along the implant from the top to the apex.

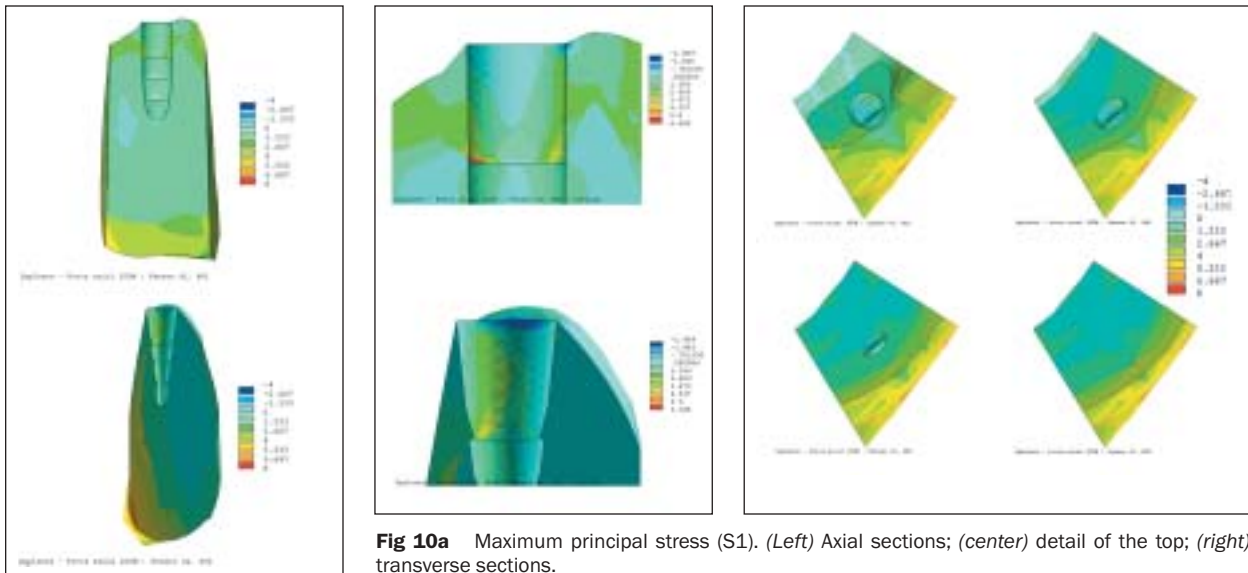


Fig 10a Maximum principal stress (S1). (Left) Axial sections; (center) detail of the top; (right) transverse sections.

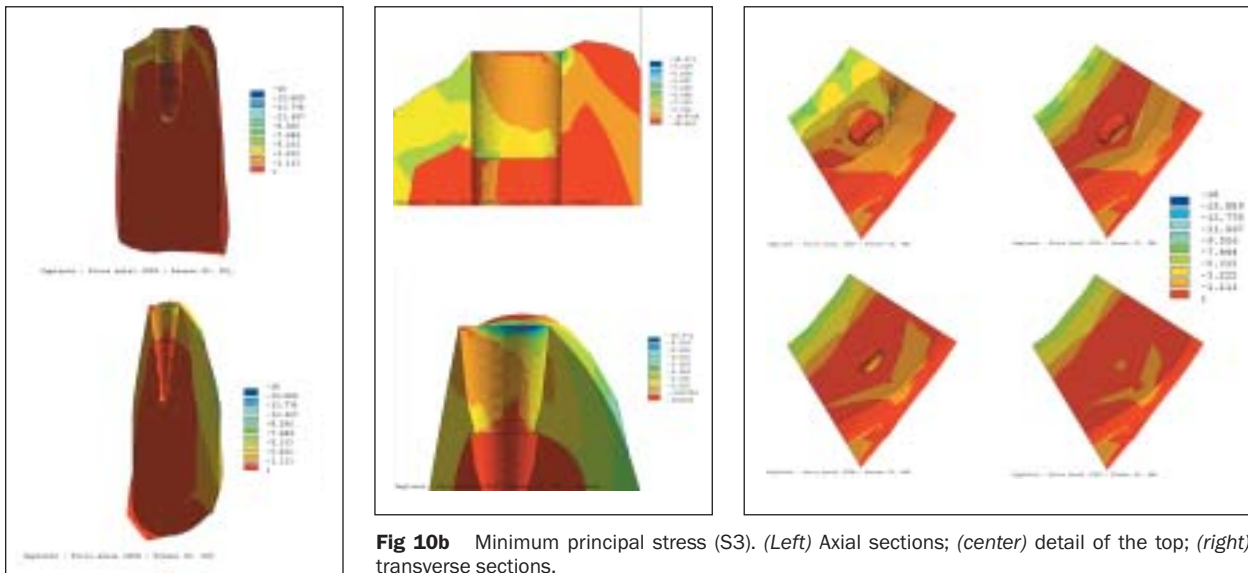


Fig 10b Minimum principal stress (S3). (Left) Axial sections; (center) detail of the top; (right) transverse sections.

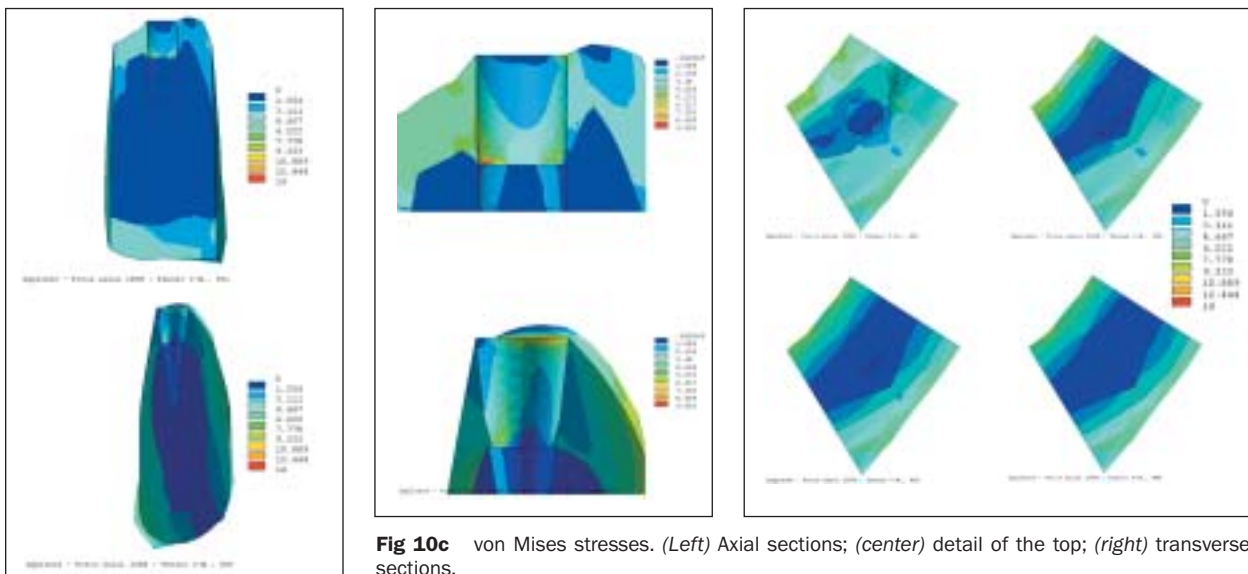


Fig 10c von Mises stresses. (Left) Axial sections; (center) detail of the top; (right) transverse sections.

DISCUSSION

In this study, the global analysis showed deformation of the mandible similar to that seen in many reports in the literature.^{38-40,47,66} The importance of this deformation in the results of FEM studies has been noted by some authors.^{38,39,42} Three-dimensional modeling^{6,38,39,43} utilizing a fine mesh with a great number of elements³⁸ contributes to the reliability of FEM.

The modeled muscular force action at the bone surface generated stresses as high as those obtained around the implant, as shown in the results. This fact provides a qualitative means of comparing the stress levels achieved and suggests that modeling of the entire mandible is important and cannot be neglected. Models with supporting systems that do not consider these factors^{11,13,28} can provide unrealistic results. A comparison of different modeling conditions can serve as a reference but does not have conclusive value. In the area around the implant, the results of the present analysis showed stress concentration in the cortical layer facing the implant neck, similar to the majority of previously reported results.^{5,7,14,15,23,49,54}

A comparison of the data obtained from this study to those obtained from 3 works presented by Rieger and coworkers,^{7,14,15} who studied different geometries modeled under the same conditions, shows that the stress concentration at the implant neck of the cuneiform-shaped implant was more favorable than that found at cylindrical and tapered threaded implants. Bone loss in this area has been correlated to this stress concentration, and some studies have used these values, together with clinical data, to confirm this statement.^{5,7,10,11,17,44,46,50,52,59} In this study, the stress concentration occurred only on one side and not around the neck as previously related.^{14,15,17,46,51,52} Rieger and coworkers¹⁵ also suggested that the cylindrical geometry analyzed in their survey, with the exception of the maximum stress found near the neck and the apex, transfers relatively low stresses to the bone along the body of the implant. This situation can lead to pathologic bone loss near the middle of the implant as a result of atrophy and at the extremities as a result of the excessive stress. The geometric contour of the implant studied demonstrated a smooth distribution of stresses and induced a gradual distribution of the load from the top to the apex region. Also, results related to other geometries have frequently described an apex stress concentration.^{5,13-15,27,34,44} In the present work, stress concentration at the apex of the implant was insignificant and probably should not be considered.

Siegele and Soltész¹³ described stress concentration at the apex of a cuneiform implant and related this to the small area at the apex of its geometry versus cylindrical implant geometry. However, the results were obtained with a nonrigid interface, ie, a nonosseointegrated implant model. Rieger and associates¹⁴ stated that tapered implants are better than cylindrical implants at avoiding punching stresses, and Rieger and coworkers¹⁵ and Sodré³⁴ related that conical geometry had better biomechanical performance. Adams¹² illustrated that a cylindrical implant design would direct most of an applied axial load to the apical region and recommended tapered geometries for better stress distribution. Deines and colleagues⁴⁵ described better performance for natural tooth geometry (ie, cuneiform) compared with other standard implant geometry.

A geometry that takes stress away from the bone crest should be chosen for clinical use, as affirmed by Akpınar and coworkers.⁴⁶ This did not totally occur with the present geometry, but the stress distribution pattern of this analysis showed values of the same magnitude at the neck and at the muscle insertion. As stated by Rieger and associates,¹⁴ low stresses can be as problematic as high stresses. In this geometry, in some areas where the stresses were very low, such as the notches in the implant body (Figs 10a to 10c), the stress values were within the limits that are sufficient to maintain normal bone physiology.^{5,7,11,53}

Because of the differences among the models used by other authors, a quantitative comparison between the different implant designs is not reasonable. However, a qualitative analysis of the presented results demonstrated that the cuneiform geometry exhibited acceptable biomechanical performance.

CONCLUSIONS

Despite the limitations of the methodology that considered the bone homogeneous, the results of static load and linear analysis support the following conclusions:

- The cuneiform-geometry implant conforms to the pattern related in the literature, with a stress concentration in the cortical region. However, the values were within the same range of the stress level in the cortex when subjected to muscular action.
- No considerable apical stress concentrations were found.
- The cuneiform geometry appeared to distribute the stress in a smooth pattern.
- The muscular action caused areas of stress concentration, suggesting that modeling of musculature is very important to the accuracy of the data obtained.

- Under muscular action, the mandible deforms in such a way that the condyles converge medially.
- The modeling methodology, conditions of the support and load system, and the finest anatomic and functional variations played important roles in the results.

ACKNOWLEDGMENTS

The authors wish to thank Dr Clóvis da Cruz Reis, whose indomitable spirit and scientific career led this work to this level. This research was funded by grants from: SEBRAE (Federal Support Service for Micro Enterprises), State Department of Minas Gerais; Maxtron, Juiz de Fora, MG, Brazil; and it was supported by the School of Engineering, Federal University of Juiz de Fora (UFJF); the Research Center for Computational Methods in Engineering (NUMEC); the Regional Center for Innovation and Technology Transference (CRITT); the Clinical Center of Research in Stomatology (CLINEST); and the National Laboratory for Scientific Computing (LNCC). The first author is a scientific consultant for the Maxtron Company.

REFERENCES

1. Brånemark P-I, Hansson BO, Adell R, et al. Osseointegrated implants in the treatment of the edentulous jaw. Experience from a 10-year period. *Scand J Plast Reconstr Surg* 1977;16 (suppl):1-132.
2. Adell R, Lekholm U, Rockler B, Brånemark P-I. A 15-year study of osseointegrated implants in the treatment of the edentulous jaw. *Int J Oral Surg* 1981;10:387-416.
3. Cook SD, Klawitter JJ, Weinstein AM. A model for the implant-bone interface characteristics of porous dental implants. *J Dent Res* 1982a;61(8):1006-1009.
4. Skalak R. Aspects of biomechanical considerations. In: Brånemark P-I, Zarb GA, Albrektsson T (eds). *Tissue-Integrated Prostheses: Osseointegration in Clinical Dentistry*. Chicago: Quintessence, 1985:117-128.
5. Rieger MR, Adams WK, Kinzel GL, Brose MO. Finite element analysis of bone-adapted and bone-bonded endosseous implants. *J Prosthet Dent* 1989a;62(4):436-440.
6. Cook SD, Weinstein AM, Klawitter JJ. A three-dimensional finite element analysis of a porous rooted Co-Cr-Mo alloy dental implant. *J Dent Res* 1982b;61(1):25-29.
7. Rieger MR, Fareed K, Adams WK, Tanquist R. A Bone stress distribution for three endosseous implants. *J Prosthet Dent* 1989b;61:223-228.
8. Brunski JB. Biomaterials and biomechanics in dental implant design. *Int J Oral Maxillofac Implants* 1988;3:85-97.
9. Brunski JB, Puleo DA, Nanci A. Biomaterials and biomechanics of oral and maxillofacial implants: Current status and future developments. *Int J Oral Maxillofac Implants* 2000;15(1):15-46.
10. Weinstein AM, Klawitter JJ, Anand SC, Schuessler R. Stress analysis of porous rooted dental implants. *J Dent Res* 1976; 55(5):772-777.
11. Borchers L, Reichart P. Three-dimensional stress distribution around a dental implant at different stages of interface development. *J Dent Res* 1983;62(2):155-159.
12. Adams VK. *Employing Finite Element Modeling in the Design Optimization of Prosthodontic Implants* [thesis]. Columbus: The Ohio State University, 1985.
13. Siegele D, Soltész U. Numerical investigations of the influence of implant shape on stress distribution in the jaw bone. *Int J Oral Maxillofac Implants* 1989;4:333-340.
14. Rieger MR, Adams WK, Kinzel GL. A finite element survey of eleven endosseous implants. *J Prosthet Dent* 1990;63(4): 457-465.
15. Rieger MR, Mayberry M, Brose MO. Finite element analysis of six endosseous implants. *J Prosthet Dent* 1990;63(4): 671-676.
16. Van Rossen IP, Braak LH, Putter C, Groot K. Stress-absorbing elements in dental implants. *J Prosthet Dent* 1990;64(2):198-205.
17. Clelland NL, Ismail YH, Zaki HS, Pipko D. Three-dimensional finite element stress analysis in and around the Screw-Vent implant. *Int J Oral Maxillofac Implants* 1991;6(4): 391-398.
18. Holmes DC, Grigsby WR, Goel VK, Keller JC. Comparison of stress transmission in the IMZ implant system with polyoximethylene or titanium intramobile element: A finite element stress analysis. *Int J Oral Maxillofac Implants* 1992; 7:450-458.
19. Mihalko WM, May TC, Kay JF, Krause WR. Finite element analysis of interface geometry effects on the crestal bone surrounding a dental implant. *Implant Dent* 1992;1:212-217.
20. Bidez MW, Misch CE. *Clinical biomechanics*. In: Misch CE (ed). *Contemporary Implant Dentistry*. St Louis: Mosby, 1993:279-311.
21. Lozada JL, Abbate MF, Pizzarello FA, James RA. Comparative three-dimensional analysis of two finite-element endosseous implant designs. *J Oral Implantol* 1994;20(4):315-321.
22. Lewinstein I, Banks-Sills L, Eliasi R. Finite element analysis of a new system (IL) for supporting an implant-retained cantilever prosthesis. *Int J Oral Maxillofac Implants* 1995;10(3): 355-366.
23. Murphy WM, Williams KR, Gregory MC. Stress in bone adjacent to dental implants. *J Oral Rehabil* 1995;22:897-903.
24. Tortamano Neto P. *Study of the Stress Transmitted to the Mandible by an Implant-supported Prosthesis Under Different Occlusal Patter by Finite Element Method* [thesis]. São Paulo, Brazil: Faculty of Dentistry, São Paulo University, 1995.
25. Van Zyl PP, Grundling NL, Jooste CH, Terblanche E. Three-dimensional finite element model of a human mandible incorporating six osseointegrated implants for stress analysis of mandibular cantilever prostheses. *Int J Oral Maxillofac Implants* 1995;10(1):51-57.
26. Baiamonte T, Abbate MF, Pizzarello F, Lozada JL, James R. The experimental verification of the efficacy of finite element modeling to dental implant systems. *J Oral Implantol* 1996;22(2):104-110.
27. Canay S, Hersek N, Akpınar I, Asik Z. Comparison of stress distribution around vertical and angled implants with finite-element analysis. *Quintessence Int* 1996;27(9):591-598.
28. Meijer HJA, Starmans FJM, Steen WHA, Bosman F. Loading conditions of endosseous implants in an edentulous human mandible: A three-dimensional, finite-element study. *J Oral Rehabil* 1996;23:757-763.
29. Papavasiliou G, Kamposiora P, Bayne SC, Felton DA. Three-dimensional finite element analysis of stress-distribution around single tooth implants as a function of bony support, prosthesis type, and loading during function. *J Prosthet Dent* 1996;76(6):633-640.
30. Vaillancourt H, Pilliar RM, Mccammond D. Factors affecting crestal bone loss with dental implants partially covered with a porous coating: A finite element analysis. *Int J Oral Maxillofac Implants* 1996;11(3):351-359.

31. Wadamoto M, Akagawa Y, Sato Y, Kubo T. The three-dimensional bone interfaces of an osseointegrated implant. I: A morphometric evaluation in initial healing. *J Prosthet Dent* 1996;76:170-175.
32. Williams KR, Williams ADC. Impulse response of a dental implant in bone by numerical analysis. *Biomaterials* 1997; 18(10):715-719.
33. Los Casas EB, Gouvêa PHP, Cornacchia TPM, Cimini CA Jr, Lanza MD. Computational modeling of dentistry problems. Proceedings of the XX CILAMCE. São Paulo:USP, 1999:1-19.
34. Sodré GSF. Dental Implant Stress Analysis Via Finite Element Method [thesis]. Belo Horizonte, Brazil: School of Engineering, Federal University of Minas Gerais, 1999.
35. Çiftçi Y, Canay S. The effect of veneering materials on stress distribution in implant-supported fixed prosthetic restorations. *Int J Oral Maxillofac Implants* 2000;15(4):571-582.
36. Gouveia PHP. Contributions for a Mechanical Behavior Model of the First Upper Bicuspid Via Finite Element Method [thesis]. Belo Horizonte: School of Engineering, Federal University of Minas Gerais, 2000.
37. Merz BR, Hunenbart S, Belser UC. Mechanics of the implant-abutment connection: An 8-degree taper compared to a butt joint connection. *Int J Oral Maxillofac Implants* 2000;15(4):519-526.
38. Knoell AC. A mathematical model of an in vitro human mandible. *J Biomech* 1977;10:159-166.
39. Koolstra JH, Van Eijden TMGJ. Application and validation of a three-dimensional mathematical model of the human masticatory system in vivo. *J Biomechanics* 1992;25(2):175-187.
40. Koriath TWP, Romilly DP, Hannam AG. Three-dimensional finite element stress analysis of the dentate human mandible. *Am J Phys Anthropol* 1992;88:69-96.
41. Keyak JH, Fourkas MG, Meagher JM, Skinner HB. Validation of the automated method of three-dimensional finite element modeling of bone. *J Biomed Eng* 1993;15:505-509.
42. Koriath TWP, Hannam AG. Deformation of the human mandible during simulated tooth clenching. *J Dent Res* 1994;73(1):56-66.
43. Inou N, Iioka Y, Fujiwara H, Maki K. Functional adaptation of mandibular bone. In: Hayashi K, Ishikawa H (eds). *Computational Biomechanics*. Tokyo: Springer-Verlag, 1996:23-42.
44. Meijer HJA, Kuiper JH, Starmans FJM, Bosman F. Stress distribution around dental implants: Influence of superstructure, length of implants, and height of mandible. *J Prosthet Dent* 1992;68(1):96-102.
45. Deines DN, Eick JD, Cobb CM, Bowles CQ, Johnson CM. Photoelastic stress analysis of natural teeth and three osseointegrated implant designs. *Int J Periodontics Restorative Dent* 1993;13(6):541-549.
46. Akpinar I, Demirel F, Parnas L, Sahin S. A comparison of stress and strain distribution characteristics of two different rigid implant designs for distal-extension fixed prostheses. *Quintessence Int* 1996;27(1):11-17.
47. Abdel-Latif HH, Hobkirk JA, Kelleway JP. Functional mandibular deformation in edentulous subjects treated with dental implants. *Int J Prosthodont* 2000;13(6):513-519.
48. Albrektsson T, Jacobsson M. Bone-metal interface in osseointegration. *J Prosthet Dent* 1987;57(5):597-607.
49. Pylant T, Triplett RG, Key MC, Brunsvold MA. A retrospective evaluation of endosseous titanium implants in the partially edentulous patient. *Int J Oral Maxillofac Implants* 1992;7(2):195-202.
50. Takuma M, Tsutsumi S, Fukunaga S, et al. Stress distribution around alumina, hydroxyapatite and plasma-sprayed titanium dental implants. *J Osaka Univ Dent Sch* 1988;28:73-82.
51. Jung Y-C, Han C-H, Lee K-W. A 1-year radiographic evaluation of marginal bone around dental implants. *Int J Oral Maxillofac Implants* 1996;11(6):811-818.
52. Stegaroiu R, Sato T, Kusakari H, Miyakawa O. Influence of restoration type on stress distribution in bone around implants: A three-dimensional finite element analysis. *Int J Oral Maxillofac Implants* 1998;13(1):82-90.
53. Hassler C, Rybicki EF, Cummings KD, Clark LC. Quantification of bone stresses during remodeling. *J Biomech* 1980; 13:185-190.
54. Hoshaw SJ, Brunski JB, Cochran GVB. Mechanical loading of Brånemark implants affects interfacial bone modeling and remodeling. *Int J Oral Maxillofac Implants* 1994;9(3):345-360.
55. Kirsch A, Mentag PJ. The IMZ endosseous two phase implant system: A complete oral rehabilitation treatment concept. *Oral Implantol* 1986;XII(4):577-585.
56. Spiekermann H. *Color Atlas of Dental Medicine: Implantology*. New York: Thieme, 1995:36-45.
57. Abu-Hammad OA, Harrison A, Williams D. The effect of a hydroxyapatite-reinforced polyethylene stress distributor in a dental implant on compressive stress levels in surrounding bone. *Int J Oral Maxillofac Implants* 2000;15(4):559-564.
58. Buser D, Warrer K, Karring T. Formation of a periodontal ligament around titanium implants. *J Periodontol* 1990;61(9):597-601.
59. Warrer K, Karring T, Gotfredsen K. Periodontal ligament formation around different types of dental titanium implants. I: The self-tapping screw type implant system. *J Periodontol* 1993;64:29-34.
60. Choi BH. Periodontal ligament formation around titanium implants using cultured periodontal ligament cells: A pilot study. *Int J Oral Maxillofac Implants* 2000;15(2):193-196.
61. Vocht JW D, Goel VK, Zeitler DL, Lew D, Hoffman EA. Development of a finite element model to simulate and study the biomechanics of the temporomandibular joint. 1999:1-9. Available at <http://everest.radiology.uiowa.edu/spie/paper10/VHPPaper.html>.
62. Posselt U. *Physiology of Occlusion and Rehabilitation*, ed 2. Oxford: Blackwell, 1964:27-79.
63. Ramfjord SP, Ash MM Jr. *Occlusion*, ed 2. Philadelphia: Saunders, 1971:60-103.
64. Graber TM. *Orthodontics: Principles and Practices*. Philadelphia: Saunders, 1972:122-168.
65. Bauer A, Gutowski A. *Gnathology*. Berlin: Quintessence, 1976:25-27.
66. Koolstra JH, Van Eijden TMGJ. The jaw open-close movements predicted by biomechanical modeling. *J Biomech* 1997;30(9):943-950.
67. Pruim GJ, Jongh HJ, Ten Bosch J. Forces acting on the mandible during bilateral static bite at different bite force levels. *J Biomech* 1980;13:755-763.
68. Cruz M, Reis CC, Silva VC. Alloplastic membrane for tissue isolation in guided tissue regeneration. *Odont Mod* 1993; 20(6):6-13.
69. Cruz M, Reis CC. Surgical repositioning of the mandibular nerve for the placement of implants. *J Clin Odont* 1998;13(2):41-50.
70. Cruz M, Reis CC, Mattos FF. Implant-induced expansion of atrophic ridges for the placement of implants. *J Prosthet Dent* 2001;85(4):377-381.